

Graphene based superconducting quantum point contacts

Ali G. Moghaddam and Malek Zareyan

Institute for Advanced Studies in Basic Sciences (IASBS), P.O. Box 45195-1159, Zanjan 45195, Iran

Received: date / Revised version: date

Abstract We investigate the Josephson effect in the graphene nanoribbons of length L smaller than the superconducting coherence length and an arbitrary width W . We find that in contrast to an ordinary superconducting quantum point contact (SQPC) the critical supercurrent I_c is not quantized for the nanoribbons with smooth and arm chair edges. For a low concentration of the carriers I_c decreases monotonically with lowering $W=L$ and tends to a constant minimum for a narrow nanoribbon with $W \ll L$. The minimum I_c is zero for the smooth edges but $I_0 \neq 0$ for the arm chair edges. At higher concentrations of the carriers this monotonic variation acquires a series of peaks. Further analysis of the current-phase relation and the Josephson coupling strength $I_c R_N$ in terms of $W=L$ and the concentration of carriers reveals significant differences with those of an ordinary SQPC. On the other hand for a zigzag nanoribbon we find that, similar to an ordinary SQPC, I_c is quantized but to the half-integer values $(n+1/2)4e I_0 \neq 0$.

1 Introduction

Graphene, a single layer graphite, is the two dimensional honeycomb lattice of carbon atoms. Recently experimental realization of graphene has introduced a new material with unique properties [1,2,3] which provide the possibility for designing new carbon based nanodevices. Most of the peculiarities come from the electronic structure of graphene which is fundamentally different from that of a metal or a semiconductor. Graphene has a gapless semimetallic band structure with a linear dispersion relation of low-lying excitations. This makes the electrons in graphene to behave identical to two dimensional massless Dirac fermions [4,5,6]. The low energy physics of electrons is then described by a two dimensional Dirac Hamiltonian acting on a four-component spinors in two

sublattice spaces of the honeycomb lattice and two independent K and K^0 points in the corresponding reciprocal lattice [7,8]. As a condensed matter counterpart of relativistic particles [9], graphene makes possible to observe early predictions like Klein paradox and zitterbewegung effect [10]. Also it has attracted an intense theoretical and experimental attention to study the effects of the relativistic-like dynamics of electrons on the different quantum transport phenomena which are already known in ordinary conducting systems.

Already several quantum transport phenomena including the integer quantum Hall effect [2,3,11], conductance quantization [12], quantum shot noise [13], and quantum tunneling [10] have been revisited in graphene and found to have anomalous features due to the relativistic like dynamics of electrons. Recently the possibility of the Josephson coupling of two superconductors by a graphene layer was considered by Titov and Beenakker [14]. Using Dirac-Bogoliubov-de Gennes formalism [15], they found that in a ballistic graphene a Josephson current can flow even in the limit of zero concentration of the carriers i.e. at the Dirac point. They found a current-phase relation $I(\phi) / I_0 = \cos(\phi/2) \text{arctanh}(\sin(\phi/2))$ with critical current depending inversely on the junction length L . These results for a wide ballistic graphene junction at the Dirac point are formally identical to those of an ordinary disordered normal metal [16,17].

The graphene Josephson junction has been studied experimentally very recently by Heersche et al. [18], and also independently Shailos et al. [19]. They have confirmed the proximity induced superconductivity in the graphene samples with superconducting electrodes at the top of them. Heersche et al. have detected a Josephson supercurrent in graphene monolayers at Dirac point with a bipolar property due to the electron-hole symmetry [18].

While the experiments and theory mentioned above had been focused on the wide graphene Josephson junctions, fabrication of graphene nanoribbons with finite widths were reported in a very recent experiment [20].

Correspondence to: zareyan@iasbs.ac.ir

Already several theoretical works have predicted important properties for graphene nanoribbons resulting from the electronic states formed at the edges [21,22,23]. So one would expect interesting properties for the graphene based junctions with different edges which introduce a new class of Josephson nanodevices.

In an ordinary superconducting quantum point contact (SQPC) shorter than superconducting coherence length it was predicted by Beenakker and van Houten [24] that the critical (maximum) supercurrent shows a step-like variation with width of the contacts of order of the Fermi wavelength of electrons. Furusaki et al. [25] considering such a system under more general assumptions obtained the same results. The quantization of the supercurrent resembles the normal conductance quantization in a ballistic quantum point contact to $2e^2/h$ times the number of the transparent quantum channels [26,27]. The quantization of the supercurrent in units of $e_0 = \pi \Delta_0$ (Δ_0 is the superconducting gap in the electrodes) was confirmed experimentally in semiconducting heterostructures [28].

In this paper we study the Josephson current in a graphene based SQPC with length L smaller than the superconducting coherence length $\xi = \hbar v_F / \Delta_0$, and an arbitrary width W , with smooth, arm chair and zigzag edges. Within the formalism of Ref. [15] we find that in contrast to an ordinary SQPC [24,25] the critical supercurrent I_c in smooth and arm chair ribbons with a low concentration of the carriers is not quantized but rather shows a monotonic decrease by lowering W . For a narrow strip $W \ll L$ the supercurrent reduces to a constant minimum which is $e_0 = \pi \Delta_0$ for arm chair edges and vanishingly small for smooth edges. We further analyze the product $I_c R_N$ (R_N being the normal resistance of the SQPC) representing the strength of the Josephson coupling, and the current-phase relations as a function of $W = L$. While the product $I_c R_N$ has a constant value of $2.08 e_0 = \pi \Delta_0$ for a wide contact $W = L$ irrespective of the edges type [14], in narrow junctions the Josephson coupling value depends on the type of the edges. By decreasing the width in smooth case, the product $I_c R_N$ decreases monotonically and reach a minimum ($= 2$) $e_0 = \pi \Delta_0$. However, in arm chair case it increases and tends to maximum of $e_0 = \pi \Delta_0$ for a narrow contact $W \ll L$. For graphene SQPC the dependence of the current-phase relation on $W = L$ is also different from an ordinary SQPC. For sufficiently narrow nanoribbons, while the smooth-edge case have a sinusoidal current-phase relation like the tunneling contacts, the arm chair-edge junction current-phase relation is $I = I_c \sin(\phi/2)$ like an ordinary SQPC.

Far from the Dirac point at high carrier concentrations, the behavior of I_c versus W consists of a similar monotonic variation and a series of peaks with distances inversely proportional to the chemical potential. We explain the absence of the supercurrent quantization as a result of the significant contribution of the evanescent modes in the supercurrent which is a unique property

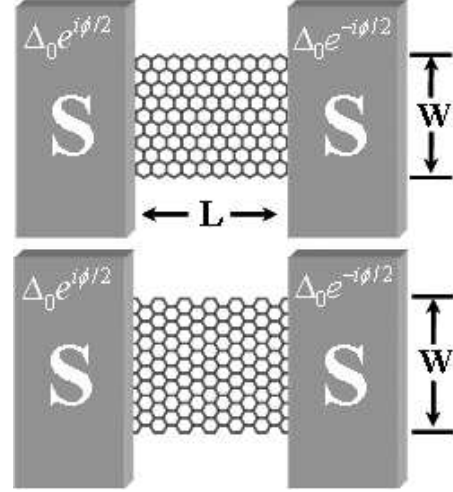


Fig. 1 Schematic of the studied junction structures. Upper (lower) panel shows a junction which has zigzag (arm chair) edges.

of graphene monolayers. Correspondingly the product $I_c R_N$ acquires an oscillatory behavior as a function of $W = \hbar v_F / \Delta_0$ with a period 2ξ . The oscillations for smooth and arm chair edges have a phase shift due to the difference in the zero-state longitudinal momenta of two cases.

For a junction with zigzag edges, because of the valley filtering characteristic [23] of the wave functions, situation is drastically different from other two edges. We find that a zigzag nanoribbon supports a half-integer quantization of the supercurrent to $(n + 1/2)4e_0 = \pi \Delta_0$ [29] with a current-phase relation identical to the ordinary SQPC.

The paper is organized as follows. In next section we introduce the model of the graphene SQPC and find the solution of the DBdG equation. In Sec. 3 we describe the boundary conditions for different edges and calculate the corresponding Josephson current. Sec. 4 is devoted to analysis of the obtained results. Finally in Sec. 5 our conclusion comes.

2 Model and basic equations

The geometry of the studied Josephson junction is shown schematically in figure 1. A ballistic graphene strip (N) connects two wide superconducting regions (S) which are produced by depositing of superconducting electrodes on top of the graphene sheets. Recent experiments have verified the reality of this model [8,19]. We assume the interfaces between the superconductors and the graphene strip are free of defects and impurities. The superconducting parts are supposed to be heavily doped such that the Fermi wavelength λ_F inside them is very smaller than the superconducting coherence length ξ and also the Fermi wavelength in the normal graphene strip λ_{FN} . By the first condition mean field theory of superconductivity will be justified and by second we can ne-

glect the spatial variation of Δ inside the superconductors close to the normal-superconductor (NS) interfaces. Thus the superconducting order parameter in the left and right superconductors has the constant values $\Delta_L = \Delta_0 \exp(i\phi_L)$, respectively, and vanishes identically in N.

The low-lying electronic states in graphene can be described by the Dirac model as linear combinations of four zero-energy Bloch functions with slowly varying envelopes $(\psi_1; \psi_2; \psi_3; \psi_4)$. Here ψ_1 and ψ_2 are the wave function components on the two inequivalent atomic sites in the honeycomb lattice usually referred as pseudospin components. The primed and unprimed functions denote the two inequivalent Dirac points K and K' in the band structure of graphene known as the two valleys. The evolution of the envelope functions is governed by the two dimensional Dirac Hamiltonian [7,8,9]:

$$\hat{H} = i\hbar v_F (\sigma_x \partial_x + \sigma_y \partial_y); \quad (1)$$

The Pauli matrices σ_x and σ_y act on the sublattice and valley degrees of freedom, respectively (with σ_x and σ_y representing the 2×2 unit matrices). The eigenfunctions of the Dirac Hamiltonian are the plane waves:

$$\begin{aligned} \psi_K &= e^{ikx + iqy} (1; e^{i\phi}; 0; 0); \\ \psi_{K'} &= e^{ikx + iqy} (0; 0; 1; e^{-i\phi}); \end{aligned} \quad (2)$$

in which the angle $\phi = \arctan(q/k)$ indicates the propagation direction. By treating the pseudospin similar to the real spin, one can easily see the pseudospin state $(1; e^{i\phi})$ aligns parallel with the propagation direction. This allows one to introduce chirality, that is formally a projection of the pseudospin on the direction of motion. The electron and hole have positive and negative chirality, respectively [10]. In ballistic systems chirality of states does not change and this conservation of chirality leads to important effects in scattering phenomena, which Klein paradox is one of them [10,15].

The superconducting correlations between the electron-hole excitations are described by the Dirac-Bogoliubov-de Gennes (DBdG) equation for the electron and hole four-component wave functions u and v [15]:

$$\hat{H} \begin{pmatrix} u \\ v \end{pmatrix} = \begin{pmatrix} \hat{H} & \Delta \\ \Delta^\dagger & -\hat{H} \end{pmatrix} \begin{pmatrix} u \\ v \end{pmatrix} = 0; \quad (3)$$

Here \hat{H} is the superconducting pair potential matrix and Δ is the time reversal operator. The excitation energy E is measured relative to the Fermi energy E_F . Each of the four blocks in Eq. 3 represents a 4×4 matrix, acting on two sublattices and two valleys spaces. The matrix form of the pair potential, and the time reversal operators are:

$$\Delta = \sigma_x \otimes \tau_0; \quad (4)$$

$$\Delta^\dagger = \sigma_x \otimes \tau_z C; \quad (5)$$

in which C is the operator of complex conjugation.

The singlet superconducting pairing always occurs between the time-reversed states. So in the case of the Dirac fermions in graphene, which the time-reversed states belong to the different valleys, the superconducting pairing is between the particles with different valleys as well as opposite spins and momenta. This causes the time reversal symmetry to play a special role in the Josephson effect compared to that in the phase coherent transport in the normal state. Indeed the presence of a superconducting electrode provides an intrinsic mechanism that couples phase coherently the electronic states belonging to the opposite valleys. So the dynamics of electrons is described by the full two-valley Hamiltonian of graphene as indicated in the DBdG equation.

The phase difference between the order parameters drives a supercurrent through the graphene strip which constitutes a weak link between two superconductors. This Josephson supercurrent is carried by the so called Andreev states which are formed in N region due to the successive conversions of the electron-hole excitations to each other (Andreev reflection) at the NS boundaries. For a short junction of length L and at zero temperature the Andreev bound (discrete) states with energies $|E| < \Delta_0$ have the main contribution to the Josephson supercurrent [24]. In this case we can neglect the contribution from the continuous states above the superconducting gap. We obtain the energies E_n of Andreev bound states by solving the DBdG equations with appropriate boundary conditions which are described below. The Josephson current is then obtained from the formula

$$I = \frac{2e}{\hbar} \frac{dF}{d\phi}; \quad (6)$$

between the Josephson current and the derivative of the free energy F with respect to the phase difference.

Inside N the solutions of the DBdG equation are independent electron and hole-like wave functions which are classified by the 2-dimensional wave vector $\mathbf{k} = (k; q)$ with the energy-momentum relation $E = \hbar v_F |\mathbf{k}|$. For a finite width W the transverse momentum q is quantized by imposing the boundary conditions at the edges. These transverse boundary conditions are different for the different edge types which a graphene strip can have.

The solutions inside the superconductors are rather mixed electron-hole excitations, called Dirac-Bogoliubov quasiparticles. The interfaces scatter the particles between the two neighboring regions. However, the excitations inside N with energy inside the gap cannot enter the superconductors and two kinds of processes, Andreev and normal reflection can occur for them. In general to match the solutions inside the different regions, one needs the scattering matrices of the interfaces. But assuming the ideal NS boundaries electron-hole scattering can be described by a longitudinal boundary condition between the electron and hole wave functions which reads [14],

$$u = \sigma_x e^{i\phi} v; \quad \phi = \arccos(E/\Delta_0) \quad (7)$$

where ϕ is the phase of ψ in S and \mathbf{n} is the unit vector perpendicular to the interface pointing from N to S.

Assuming elastic processes, scattering at the interfaces does not change the transverse momentum q and there is not any scattering between the different modes. So the Andreev states will be linear combinations of the wave functions from the same mode n with certain transverse momentum q_n . For each type of the edges by imposing the longitudinal boundary conditions at the interfaces to a general linear combination of the electron and hole states of mode n we reach to an equation for the Andreev energies $E_n(\phi)$. Throughout the paper we will consider the limit $\phi = 0$ where the retro-Andreev reflection dominates [5]. In this regime the longitudinal momenta of the electron and hole $k_n(\phi)$ can be approximated with $k_n(0)$ independent of the excitation energy [14].

3 Josephson current of the nanoribbons with different edges

3.1 Smooth edges

A graphene strip with smooth edges corresponds to an infinite mass confinement which is described by the following boundary conditions [30],

$$\psi_1(0) = \psi_2(0); \quad \psi_1(W) = \psi_2(W); \quad (8)$$

These conditions do not mix the two valleys and we can treat them independently. By this conditions the transverse momentum is obtained to have the quantized values $q_n = (n + \frac{1}{2})\pi/W$. We note that this quantization condition for the Dirac particles confined by an infinite mass differs from the corresponding one for the ordinary normal electrons by a offset of $1/2$. This originates from the Berry phase $\phi_B = \pi$ in monolayer graphene which cause phase shift in the boundary conditions as well [3, 30]. Considering a linear combination of the plane wave solutions (Eq. 2) with opposite transverse momenta and applying the boundary conditions we can find the modes inside the strip. The electron modes for each valley are indicated by the wave functions of the form :

$$\psi_k = e^{ikx} [\sin(qy - Et); \sin(qy + Et)]: \quad (9)$$

The hole wave functions ψ_k for each particular mode are the time reversed of the corresponding electron mode. Andreev bound states for each mode will be a linear combination of ψ_k and ψ_{-k} :

$$\psi_A = \frac{u_A}{v_A} = \frac{a u_k + b u_{-k}}{a v_k + b v_{-k}} : \quad (10)$$

To form an Andreev state this general form should satisfy the longitudinal boundary conditions (Eq. 7) at the NS interfaces ($x = 0; L$). These conditions result in four independent homogeneous equations for four coefficients.

By solving these equations we obtain the quantized Andreev energy as

$$E_n(\phi) = 0 \pm \frac{q_n}{t_n} \sin^2(\phi/2); \quad (11)$$

with $t_n = [1 + (q_n/k_n)^2 \sin^2(k_n L)]^{-1}$. Comparison with Ref. [13] shows that t_n is indeed the transmission probability for a ballistic smooth-edge strip of graphene between two heavily doped electrodes in the normal state. This type of relation between the Andreev energies and normal-state transmission probabilities t_n is a universal form in the short junction limit ($L \ll \lambda_F$) [24]. By means of this method we can also find the transparency of each mode and then calculate the normal state conductance (G_N) using the Landauer-Buttiker formula at zero temperature:

$$G_N = R_N^{-1} = 4 \frac{e^2}{h} \sum_n t_n : \quad (12)$$

The factor 4 at above relation accounts for the two-fold spin and valley degeneracies. Now from the Andreev energies and also Eq. 6 the Josephson current at zero temperature can be found.

Let us concentrate on the transmission coefficients and their dependence on the size and geometry of the junction. We note that in general both types of oscillatory (real k_n) and evanescent (imaginary k_n) modes participate in the transport. The number of propagating modes is limited by the width as compared to the Fermi wavelength. Indeed only the modes with $n \leq N_W = W/\lambda_F \approx 1/2$ can propagate and all the upper states are evanescent. Such a distinction between the modes exists in an ordinary QPC but with an important difference. In the QPC the transparencies depend on the longitudinal kinetic energy $E_n^k = \hbar^2 k_n^2/2m$ as $t_n = 1/(1 + e^{E_n^k})$, in which λ_F is a function of the geometry and size of the channel [31, 32]. Because of the quadratic form of the dispersion relation and high Fermi energies in comparison with λ_F , we have $t_n^k = 1$ for all modes. Consequently all the propagating modes are completely transmitted and the evanescent modes have very small transparencies. But since in graphene very small Fermi energies are accessible and the energy depends linearly on the momentum the evanescent modes can have a significant contribution in the transport. In particular near the Dirac point $L \approx \lambda_F/2$, the number of propagating modes are very small and the evanescent modes have the main contribution in the transport. This is the unique property of the graphene Josephson junctions in which very small Fermi energies are accessible. In this limit the transmission coefficients through ballistic graphene are approximately,

$$t_n = \cosh^{-2}(q_n L); \quad (13)$$

which have the same form as transmission eigenvalues of the diffusive transport through a disordered contact [33].

3.2 Arm chair edges

From Fig. 1 (lower panel) one may see that at the arm-chair edges the termination consists of a line of dimers. Therefore the wave function amplitude vanishes on both sublattices at the two edges. This leads to the boundary conditions,

$$\psi_1 = 0; \quad \psi_2 = 0 \quad (14)$$

at the both edges. In contrast to the smooth edges, arm-chair edges mix the two valleys and causes scattering of a wave propagating on a certain valley to the opposite valley. The boundary conditions leads to the quantized transverse momenta $q_n = n\pi/W$ similar to the usual confinement of normal electrons. Due to the valley changing property of these edges, the electron wave function of each mode inside the nanoribbon is a mixture of the two valleys with the form

$$u = e^{ikx} [e^{iqy} (1; e^i); e^{-iqy} (1; e^i)]: \quad (15)$$

This wave function has the same chirality for both valleys contributions, as a result of the symmetric boundary conditions. Also one should note that in contrast to the smooth edges, the wave functions $u(q)$ and $u(-q)$ represent distinct solutions in which the components of the two valleys are interchanged. As a result the lowest mode $n = 0$ has not the two fold valley degeneracy of the higher $n = 1; 2; \dots$ modes. This zero mode with zero transverse momentum can exist inside the channel even if its widths becomes smaller than the Fermi wavelength. Like the case of the smooth edges the Andreev state wave function corresponding to a given mode n is the combination of u_K and v_K . But there is a difference with the smooth case. This time u_A and v_A have four nonzero components. Applying the longitudinal boundary conditions leads to 8 equations for the coefficients a, b, c, d in Eq. 10. However because of the symmetry between the contributions from the two valleys, only 4 of them are independent. We find that the Andreev energies have the same form as in the smooth strip (Eq. 11). So we would expect to reach similar results for I_c and G_N as well.

3.3 Zigzag edges

We now consider the case of the zigzag edges. It is clear from Fig. 1 (upper panel) that atoms at zigzag edges belong to different sublattices. The boundary conditions are $\psi_1 = 0 = \psi_2$ at $y = 0$ and $\psi_1 = 0 = \psi_2$ at $y = W$ [34], which lead to the transcendental relation,

$$\sin(qW) = qW = \pi W / \lambda_F = (\pi + \epsilon)W; \quad (16)$$

for the transverse momentum q . In contrast to the previous cases this relation couples q to the excitation energy ϵ . Of course in the regime of our interest ($\epsilon \ll \epsilon_0$) we can neglect ϵ at Eq. 16. This equation has a finite

number of solutions depending on the value of $W = \pi \lambda_F$. Indeed all possible values of the transverse momenta are smaller than $\pi \lambda_F$ and thus the longitudinal momenta always have real values. This means that all the modes inside the nanoribbon with zigzag edges are propagating. For $W = \pi \lambda_F < 1$ there is an imaginary solution q labeling an evanescent mode in the y -direction. In the interval $1 < W = \pi \lambda_F < 3/2$, the transcendental relation has a single oscillatory solution. For larger $W = \pi \lambda_F$ the number of the solutions increases by two whenever the width is increased by a half of the Fermi wavelength $\lambda_F = \hbar v_F / \epsilon$. We classify the wave functions to two groups according to the signs in the transcendental relation. To find the wave functions we consider the general combination of the plane wave solutions:

$$u = A e^{iq_K} + B e^{-iq_K} + A^0 e^{iq_0} + B^0 e^{-iq_0}; \quad (17)$$

The boundary condition at $y = 0$ leads to $A + B = A^0 + B^0 = 0$. So the wave function must be as below:

$$u = e^{ikx} \begin{pmatrix} A \sin(qy) \\ B \sin(qy) \\ A^0 \sin(qy) \\ B^0 \sin(qy) \end{pmatrix} \quad (18)$$

Now to satisfy the second condition at $y = W$ there are two ways. We can have either $\sin(qW + \epsilon) = 0$ and $A^0 = 0$ or $\sin(qW - \epsilon) = 0$ and $A = 0$. We consider the solutions belonging to the group with $\sin(qW) = qW = \pi \lambda_F = W$. If k is positive the first way for satisfying the boundary conditions will be possible and if k is negative then the second way is acceptable. So the electronic wave functions of the first group (+ sign) have the forms,

$$u^+ = e^{ikx} [\sin(qy); \sin(qy + \epsilon); 0; 0]; \\ u^- = e^{-ikx} [0; 0; \sin(qy); \sin(qy - \epsilon)]; \quad (19)$$

which, respectively, describe a right-going wave on the valley K and a left-going wave in the other valley K^0 . It can be easily seen that the wave functions of the second group (- sign) are obtained from the above functions by the replacement $k \rightarrow -k$. We note that for each mode the zigzag nanoribbon operates as a valley filter for the waves with mixed valley components [23]. Since the valley index and q are conserved upon a normal reflection, the filtering property prevents the electrons from such scattering. Consequently the wave function of each bound state in N will be a combination of u^+ and v^+ . From the longitudinal condition (Eq. 7) we obtain that the energy of the Andreev state does not depend on the transverse mode n and is given by,

$$\epsilon = \epsilon_0 \cos(\pi/2); \quad (20)$$

which is the same as the Andreev energies of an ordinary SQPC [24].

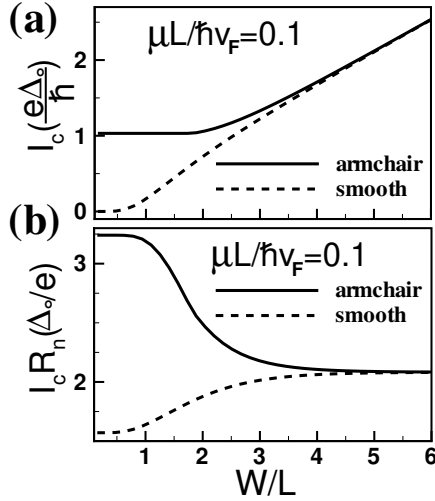


Fig. 2 The critical current (a) and the product $I_c R_N$ (b) dependence on the relative width of junction at a typical small value $\mu L/\hbar v_F = 0.1$ for smooth and arm chair strips.

4 Results and discussion

Let us first consider the behavior of the Josephson current near the Dirac point when $\mu L/\hbar v_F \ll 1$. Fig. 2 shows the critical current and the product $I_c R_N$ variations with $W=L$ for the smooth and arm chair edges at a typical small Fermi energy $\mu L/\hbar v_F = 0.1$. We see I_c has a linear dependence on $W=L$ at large $W=L$ (2a) which is the result of diffusive-like transport in the ballistic graphene [14]. By decreasing $W=L$, the transmission probabilities of the modes through N decrease and the critical current shows a monotonic decrease without any quantization. For a narrow strip $W \ll L$ the evanescent modes transparencies are vanishingly small and I_c reduces to a constant minimum value. For the smooth edges there is no propagating mode when $W < (\pi/2)\hbar v_F$ and the minimum supercurrent is vanishingly small. However in the case of the arm chair edges a lowest nondegenerate mode with $q = 0$ always can propagate irrespective of the width of the junction. This zero mode results in a bound state carrying a nonzero residual supercurrent $I_c = e_0 \sim$ for $W \ll L$. (Fig. 2a)

For a wide contact the normal state conductance G_N has the same linear dependence on $W=L$ as I_c and thus the product $I_c R_N$ reaches a constant value $2.08 e_0 = e$ in the limit $W \ll L$ (see Fig. 2b) for both types of the edges. Decreasing the width the difference between the Josephson coupling constants of the junctions with two different edges appears. For smooth (arm chair) edges $I_c R_N$ decreases (increases) monotonically with lowering $W=L$ and reaches to a minimum (maximum) of $(1/2) e_0 = (e/2)$ for a narrow junction of $W \ll L$ (see Fig. 2b).

As indicated in Fig. 3 the current-phase relation of finite-width junction differs significantly for the arm chair and smooth cases specially for very narrow strips. However at the limit of very wide junctions $W \gg L$ for both

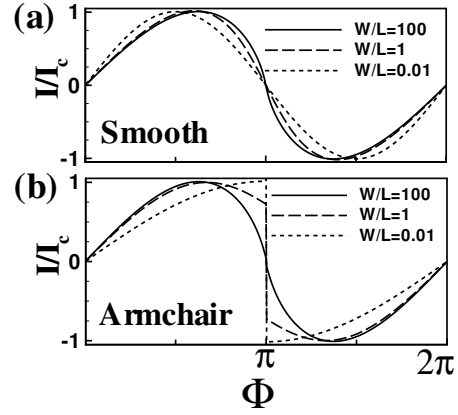


Fig. 3 The current-phase relation for junctions with smooth and arm chair edges at different $W=L$ values for $\mu L/\hbar v_F = 0.1$.

types, the current-phase relation is like a diffusive metal junction [16,17]:

$$I(\phi) = \frac{e_0 2W}{L} \cos(\phi/2) \operatorname{arctanh}(\sin(\phi/2)): \quad (21)$$

On the other hand a very narrow strip $W \ll L$ with smooth edges has a sinusoidal current-phase relation $I(\phi) = I_c \sin(\phi)$ similar to a tunnel Josephson junction. This is expected as in this limit the transmission probabilities are very small and the graphene ribbon behaves as a tunnel junction. For a narrow arm chair ribbon the current-phase relation reads

$$I = I_c \frac{\cos(\phi/2)}{j \cos(\phi/2) j} \sin(\phi/2) \quad (22)$$

which is the characteristic relation for the SQPC. This is also understandable because even in a very narrow arm-chair strip there is a propagating mode with complete transmission which makes it similar to the SQPC. The current-phase relation of smooth and arm chair junctions are shown in Fig. 3 for different $W=L$.

Now let us consider the Josephson current at a higher Fermi energy far from the Dirac point. Fig. 4a and 4b show the dependence of I_c and $I_c R_N$ on the junction width, respectively, for $\mu L/\hbar v_F = 5$. In this regime both the propagating and evanescent modes contribute to the supercurrent. Roughly speaking the amplitude of the contribution from the evanescent modes is proportional to $W=L$, however, the propagating modes contribution is proportional to their number $N_W \propto W = \hbar v_F \cdot W$ when $\mu L/\hbar v_F \gg 1$, the evanescent modes play the main role in the transport and thus the transport is diffusive-like and both the critical current and conductance are proportional inversely to length of the junction L . On the other hand, when $\mu L/\hbar v_F \ll 1$ the propagating modes have the major contribution. This cause that the envelope of the critical current depends linearly on $W \propto \hbar v_F$. In addition to this overall increase with $W \propto \hbar v_F$ the

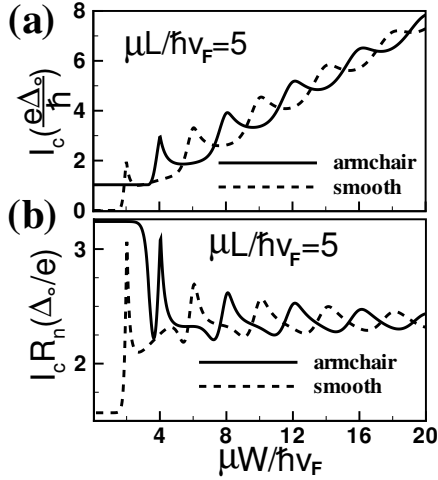


Fig. 4 The critical current (a) and the product $I_c R_N$ (b) dependence on the relative width of junction at a typical large value $\mu L/\hbar v_F = 5$ for smooth and arm chair strips.

critical current undergoes a series of peaks which become smoother by increasing $W/\hbar v_F$. Each peak (jump) signals addition of a new propagating mode in the transport when the width increases by a Fermi wavelength. Both the critical current and the product $I_c R_N$ have an oscillatory behavior versus $W/\hbar v_F$ with a period of 2 (Fig. 4). We should note that due to a nonzero transverse momentum of the lowest mode ($n = 0$) in the junction with smooth edges (while the zero mode of the arm chair-edge nanoribbon has zero transverse momentum), the oscillations are shifted by half a period with respect to those of the arm chair edges case. Also comparing the results of Fig. 2 and 4, we see that the limiting values of I_c and $I_c R_N$ at $W \rightarrow L$ is always the same and does not depend on the value of the chemical potential. Therefore we find that for these two types of the edges there is no sharp quantization and stepwise variation with width for I_c and G_N . This is again a unique property of graphene with smooth and arm chair edges in which the evanescent modes can contribute significantly in the transport.

Finally let us analyze the Josephson supercurrent for the zigzag ribbon. As we argued in section 3 in this case the valley filtering nature of the wave functions in NP prevents the normal reflections at NS interfaces. In addition, because of the transcendental relation of the transverse momenta which connects their values by the Fermi energy, there is no evanescent mode with imaginary k and the situation is similar to an ordinary SQPC. The critical supercurrent shows a step-wise variation with

$W/\hbar v_F$ but with the following important anomalies (see Fig. 5). In contrast to an ordinary SQPC [24,25], the width of the first step ($3=4$) is bigger than that of the higher steps ($1=2$). The extra width is the contribution of the single y -directional evanescent mode (imaginary q) for $W < \hbar v_F$. Also the height of the first step is $1=2$ of the height of the higher steps which itself is four

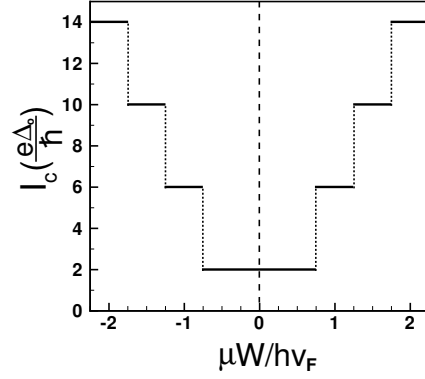


Fig. 5 The critical current vs. relative width of junction which has zigzag edges.

times bigger than $e_0 \approx$ the supercurrent quantum in an ordinary SQPC. Therefore the supercurrent through a zigzag graphene nanoribbon is half-integer quantized to $(n + 1/2)4e_0 \approx$. The effect resembles the conductance quantization in graphene strips with zigzag edges [12] and also the half-integer Hall effect [2,3,11] in monolayer structures. From expression of the Andreev energies for the zigzag junction (Eq. 20) we find that the current-phase relation is given by Eq. 22 similar to an ordinary SQPC with length smaller than L .

5 Conclusion

In conclusion we have investigated the Josephson effect in a short graphene nanoribbons of width W and length $L \gg \ell_0$ connecting two heavily doped superconducting electrodes. Within a Dirac-Bogoliubov-de Gennes formalism, we have found that the variation of the Josephson supercurrent versus the width W is drastically different for different types of edges. In the smooth and arm chair nanoribbons with low concentration of the carriers the critical supercurrent I_c decreases monotonically by decreasing W/L . For a narrow strip $W \ll L$ with arm chair and smooth edges, I_c takes constant minimum $e_0 \approx$ and 0, respectively. The Josephson coupling strength given by the product $I_c R_N$ has been found to have a minimum $(1=2)e_0$ (maximum e_0) for a narrow junction $W \ll L$ with smooth (arm chair) edges and increases (decreases) monotonically with W/L to reach the wide junction value $2.08 e_0$. We have also seen the different dependence of the current-phase relation on W/L for junctions with the two different edge types.

For the higher concentration of the carriers, the overall monotonic dependence of I_c acquires a series of peaks with distances inversely proportional to the chemical potential. Correspondingly the product $I_c R_N$ shows an oscillatory behavior with $W/\hbar v_F$ with a period of 2. The oscillations for smooth and arm chair edges are phase shifted by π .

For the zigzag edges the results are quite different due to the special quantization relation of transverse momenta and the valley filtering property of the electron wave functions. We have found a step-wise variation of I_c versus $W = \hbar v_F$, implying a half-integer quantization of the supercurrent to $(n + 1/2)4e_0 = \sim$. The current-phase relation is found to be similar to an ordinary superconducting quantum point contact.

Acknowledgments

One of the authors (M. Z.) thanks A. B. Rataas for his hospitality and support at the Center for Advanced Study, Oslo where parts of this work were done.

References

1. K. S. Novoselov, A. K. Geim, S. V. Morozov, D. Jiang, Y. Zhang, S. V. Dubonos, I. V. Grigorieva, A. A. Firsov, *Science* 306, 666 (2004).
2. K. S. Novoselov, A. K. Geim, S. V. Morozov, D. Jiang, M. I. Katsnelson, I. V. Grigorieva, S. V. Dubonos, A. A. Firsov, *Nature* 438, 197 (2005).
3. Y. Zhang, Y. W. Tan, H. L. Stormer, P. Kim, *Nature* 438, 201 (2005).
4. P. R. Wallace, *Phys. Rev.* 71, 622 (1947).
5. J. C. Slonczewski, P. R. Weiss, *Phys. Rev.* 109, 272 (1958).
6. G. W. Semenoff, *Phys. Rev. Lett.* 53, 2449 (1984).
7. D. P. DiVincenzo, E. J. Mele, *Phys. Rev. B* 29, 1685 (1984).
8. T. Ando, *J. Phys. Soc. Jpn.* 74, 777 (2005).
9. F. D. M. Haldane, *Phys. Rev. Lett.* 61, 2015 (1988).
10. M. I. Katsnelson, K. S. Novoselov, A. K. Geim, *Nature Phys.* 2, 620 (2006).
11. V. P. Gusynin, S. G. Sharapov, *Phys. Rev. Lett.* 95, 146801 (2005).
12. N. M. R. Peres, A. H. Castro Neto, F. Guinea, *Phys. Rev. B* 73, 195411 (2006).
13. J. Tworzydło, B. Trauzettel, M. Titov, A. Rycerz, C. W. J. Beenakker, *Phys. Rev. Lett.* 96, 246802 (2006).
14. M. Titov, C. W. J. Beenakker, *Phys. Rev. B* 74, 041401(R) (2006).
15. C. W. J. Beenakker, *Phys. Rev. Lett.* 97, 067007 (2006).
16. C. W. J. Beenakker, *Phys. Rev. Lett.* 67, 3836 (1991); 68, 1442(E) (1992).
17. I. O. Kulik, A. N. Omelyanchuk, *Pisma Zh. Eksp. Teor. Fiz.* 21, 216 (1975); *JETP Lett.* 21, 96 (1975).
18. H. B. Heersche, P. Jarillo-Herrero, J. B. Oostinga, L. M. K. Vandersypen, A. F. M. Morpurgo, *Nature* 446, 56 (2007).
19. A. Shailos, W. Nativel, A. Kasumov, C. Collet, M. Ferrier, S. Gueron, R. Deblock, H. Bouchiat, *Europhys. Lett.* 79, 57008 (2007).
20. Z. Chen, Y.-M. Lin, M. J. Rooks, P. A. Vouris, *Physica E* 40, 228 (2007).
21. Y.-W. Son, M. L. Cohen, S. G. Louie, *Nature* 444, 347 (2006).
22. Y.-W. Son, M. L. Cohen, S. G. Louie, *Phys. Rev. Lett.* 97, 216803 (2006).
23. A. Rycerz, J. Tworzydło, C. W. J. Beenakker, *Nature Physics* 3, 172 (2007).
24. C. W. J. Beenakker, H. van Houten, *Phys. Rev. Lett.* 66, 3056 (1991).
25. A. Furusaki, H. Takayanagi, M. Tsukada, *Phys. Rev. Lett.* 67, 132 (1991); *Phys. Rev. B* 45, 10563 (1992).
26. B. J. van Wees, H. van Houten, C. W. J. Beenakker, J. G. Williamson, L. P. Kouwenhoven, D. van der Marel, C. T. Foxon, *Phys. Rev. Lett.* 60, 848 (1988).
27. A. Wharam, T. J. Thornton, R. Newbury, M. Pepper, H. Ahmed, J. E. Frost, D. G. Hasko, D. C. Peacock, D. A. Ritchie, G. A. C. Jones, *J. Phys. C* 21, L209 (1988).
28. H. Takayanagi, T. Akazaki, J. Nitta, *Phys. Rev. Lett.* 75, 3533 (1995).
29. A. G. Moghaddam, M. Zareyan, *Phys. Rev. B* 74, 241403(R) (2006).
30. M. V. Berry, R. J. Mondragon, *Proc. R. Soc. Lond. A* 412, 53 (1987).
31. L. I. Glazman, G. B. Lesovik, D. E. Khmel'nitskii, R. I. Shekhter, *JETP Lett.* 48, 238 (1988).
32. M. Buttiker, *Phys. Rev. B* 41, 7906 (1990).
33. A. D. Stone, P. A. Mello, K. A. Muttalib, J.-L. Pichard, in *Mesoscopic Phenomena in Solids*, edited by B. L. Altshuler, P. A. Lee, and R. A. Webb (North-Holland, Amsterdam, 1991).
34. L. Brey, H. A. Fertig, *Phys. Rev. B* 73, 235411 (2006).